ARTICLE

Fluorescence Emission Mediated by Metal-Dielectric-Metal Fishnet Metasurface: Spatially Selective Excitation and Double Enhancement

Yuan Ren, Yong-hua Lu*, Tian-yang Zang, Sonia Ghafoor, Pei Wang*

Department of Optics and Optical Engineering, Anhui Key Laboratory of Optoelectronic Science and Technology, University of Science and Technology of China, Hefei 230026, China

(Dated: Received on July 31, 2018; Accepted on August 13, 2018)

Enhancement of fluorescent radiation is of great importance for applications including biological imaging, high-sensitivity detectors, and integrated light sources. Strong electromagnetic fields can be created around metallic nanoparticles or in gap of nanostructures, where the local state density of radiating mode is then dramatically enhanced. While enhanced fluorescent emission has been demonstrated in many metallic nanoparticles and nanoparticle pairs, simultaneous mediation of absorption and emission processes of fluorescent emitters remains challenging in metallic nanostructures. Here, we investigate fluorescent emission mediated by metal-dielectric-metal fishnet metasurface, in which localized surface plasmon (LSP) and magnetic plasmon polaritons (MPPs) modes are coupled with absorption and emission processes, respectively. For absorption process, coupling of the LSP mode enables spatially-selective excitation of the fluorescent emitters by rotating the polarization of the pump laser beam. In addition, the polarization-dependent MPP mode enables manipulation of both polarization and wavelength of the fluorescent emission by introducing a rectangular fishnet structure. All the experimental observations are further corroborated by finite-difference time-domain simulations. The structure reported here has great potential for application to color light-emitting devices and nanoscale integrated light sources.

Key words: Surface plasmons, Fluorescence emission enhancement, Spectroscopy modulation, Metasurface

I. INTRODUCTION

Engineering spontaneous emission of fluorophores using metallic nanostructures is among the most prosperous and promising research fields in plasmonics [1–3]. The capability to confine light within a nanoscale volume is of major importance to enable efficient change in the local electromagnetic environment, thus providing enhancement [4] or suppression [5] of the fluorescent emission. Metallic nanostructures such as single nanoparticles [6, 7], metallic pairs [8–10], and periodic metallic arrays [11], have been fabricated to provide enhanced fluorescent emission using localized surface plasmon (LSP). Furthermore, coupling between nanoscale metallic elements or arrays also provides a variety of localized electromagnetic modes, such as gap mode [12–14], lattice mode [15, 16], and magnetic plasmon polaritons (MPPs) [17–20]. The control of fluorescence via multi-mode resonances in plasmonic metasurface has been widely studied. These plasmon-enhanced fluorescence and absorption processes for molecules have an extensive range of potential applications, including optical sensors [21, 22], biological imaging [23, 24], light-emitting devices [25, 26], and solar energy harvesters [27].

To provide prominent enhancement, the size or gap of a nanoantenna structure must be carefully adjusted to ensure that the plasmonic resonance wavelength matches the fluorescent radiation spectrum. Coupling with plasmonic mode can modify efficiency [28], polarization [29] and directivity [30] of the fluorescent emission. Typical works in this field emphasize only the control of the emission process with plasmonic resonance [31, 32]. However, for photoluminescence, coupling between the pump laser beam and the plasmonic resonance also contributes to enhancement of fluorescent radiation [33]. One possible way to enhance both excitation and radiation of the emitter is to adopt a broad plasmonic resonance that overlaps the emitter's excitation and radiation spectra simultaneously [34]. Another preferable solution is to design metallic nanostructures that have multiple resonance modes corresponding to the fluorescence absorption and emission spectra [35], which will then provide greater freedom for manipulation of the radiation of fluorescent emitters.

In this work, the photoluminescence of Nile Red molecules buried in metal-dielectric-metal (MDM) fish-

*Authors to whom correspondence should be addressed. E-mail: yhlu@ustc.edu.cn, wangpei@ustc.edu.cn

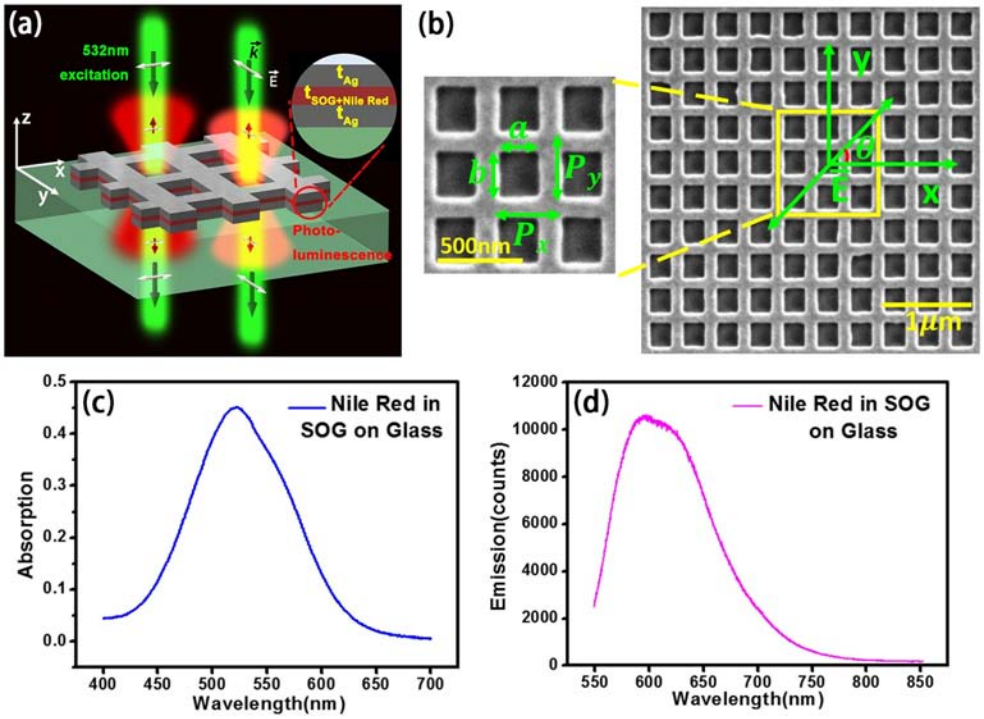

FIG. 1 MDM fishnet material. (a) Schematic of the fishnet structure. (b) Scanning electron microscopy image of the fabricated structure. (c) Absorption and (d) photoluminescence emission spectra of Nile Red molecules mixed in SOG solution and then spin-coated on glass substrate.

net nanostructures is enhanced by matching both the excitation and radiation wavelengths with the LSP and MPP modes, respectively. We demonstrate that the spatial electromagnetic distributions of these two modes are of major importance to acquire enhanced fluorescent emission. Because the spatial distribution of LSP mode is dependent on the polarization of excitation laser, the fluorophores can be spatially-selectively excited by rotating the polarization of the pump laser beam; therefore, the wavelength and the polarization of the enhanced fluorescence can be manipulated using MPP mode. The results of finite-difference time-domain (FDTD) simulations of the electromagnetic characteristics of the MDM fishnet metasurface support all the experimentally measured results.

II. SAMPLE PREPARATION

FIG. 1(a) shows a schematic of the MDM fishnet metasurface used to manipulate the photoluminescence of Nile Red molecules sandwiched in the gap. The MDM fishnet metasurface was fabricated by perforation of rectangular holes in MDM films that were deposited on a glass substrate (the refractive index of glass substrate is 1.518). The top and bottom silver films, which have the same thickness t_{Ag}, were deposited by evaporation, while the gap dielectric film was spin-coated spin-on glass (SOG; IC1-200, Futurrex), with Nile Red fluorescent molecules (Sigma) dispersed within the film to act as dipolar emitters (the dielectric film has a thickness denoted by t_{SOG} with a refractive index of 1.41). The concentration of Nile Red molecules in the SOG layer was 5×10^{-4} mol/L. The resist was diluted in n-butanol at a ratio of 1:8.5 and spun on at 5000 r/min with an acceleration of 1000 r·min^{-1}·s^{-1} for 40 s, and the mixture was then baked at 120°C for 1 min to remove the solvents. To create a periodic pattern of rectangular apertures passing through the stack of three alternating silver and SOG films, the focused ion beam (FIB; FEI Helios NanoLab 650) milling technique was used. The fluorophores were excited by linearly polarized incident light with its polarization oriented at an angle of θ relative to x-axis. FIG. 1(b) shows a scanning electron microscopy (SEM) image of the MDM fishnet structure with t_{Ag}=35 nm, t_{SOG}=30 nm, hole length a=220 nm, width b=255 nm, and rectangular lattice constants of P_x=365 nm and P_y=370 nm. FIG. 1 (c) and (d) show the absorption and photoluminescence emission spectra of Nile Red molecules which are mixed in SOG solution and then spin-coated on glass substrate, respectively. The absorption spectrum (FIG. 1(c)) was measured by using a commercial UV-2550 PC spectrometer (Shimadzu) with a broadband white illumination (wavelength ranges from 190 nm to 1100 nm), which peaks at wavelength of 523 nm. The photoluminescence emission spectrum (FIG. 1(d)) was measured with an excitation wavelength of 532 nm (ex-

DOI:10.1063/1674-0068/cjcp1807182

citation power is 300 μW, acquisition time is 0.2 s), which peaks at 600 nm and extends to 800 nm although the fluorescent emission intensity decays a lot for wavelengths longer than 700 nm. All the geometric parameters of this structure were chosen to ensure compatibility between the electromagnetic resonant modes of the nanostructure and the absorption and emission spectra of the emitters.

III. MULTIPLE RESONANT MODES

As previously demonstrated, multiple plasmonic resonant modes occur in MDM fishnet metasurfaces, including LSP, MPP, and surface plasmon polariton-Bloch waves (SPP-BWs). The resonant wavelengths of these modes can be tuned by modifying the geometric sizes of the fishnet lattice structure. To identify the resonant modes of the lattice sample (FIG.1(b)), polarization-dependent transmittance spectra were measured in visible wavelength between 500 nm and 800 nm using a local spectra detection setup. Linearly-polarized white light was used to provide normal illumination of the sample. The transmitted light was then collected using an objective lens (60×, NA=1.42, Olympus) and recorded using an automated imaging spectrometer (Jobin Yvon iHR550). All the transmission spectra were normalized with respect to the background spectrum of glass substrate. FIG. 2(a) gives the transmittance spectrum of the MDM fishnet device under illumination by x-polarized incident light and FIG. 2(b) shows the corresponding spectrum for y-polarized incident light. The dips located at λ_{1x}=520 nm for x-polarization and λ_{1y}=505 nm for y-polarization are attributed to LSP mode, while the dips located at λ_{2x}=598 nm and λ_{2y}=616 nm are attributed to SPP-BWs mode. Because the periods of the fishnet lattice along x- and y-axes are approximately equal, LSP and SPP-BWs wavelengths are almost independent of the polarization of the incident light. Notable blueshift in the magnetic resonance wavelength is observed when the polarization of incident light is changed from an x-orientation (λ_{3x}=714 nm) to a y-orientation (λ_{3y}=650 nm) because length and width of the air hole are very different while the lattice periods along x- and y-axis are almost equal.

The presence of these multiple resonant modes is further corroborated using three-dimensional finite-difference time-domain simulation (FDTD solutions, Lumerical Solutions Ltd.). In this case, the dielectric coefficient used for Ag was taken from Palik's data (0–2 μm) [36]. The transmitted spectra were monitored at a plane located 1 μm below the sample surface. The simulated transmission spectra for an MDM fishnet metasurface with same geometric parameters as the fabricated sample are shown in FIG. 2(c) for x-polarization and FIG. 2(d) for y-polarization. All the resonant dips are located at exactly the same wavelengths as that of the experimental measurements. In addition, the localized electromagnetic field distributions of LSP mode for x-polarization (FIG. 2(f)) and y-polarization (FIG. 2(g)) are recorded in the gap (Plane A in FIG. 2(e)). While the distributions of MPP mode were recorded in Plane B (FIG. 2(h)) for x-polarization and in Plane C (FIG. 2(h)) for y-polarization. FIG. 2(i) presents the electric field distribution of MPP(x) mode recorded in Plane B and FIG. 2(j) for MPP(y) recorded in Plane C. The color in the map indicates the field magnitude while the arrows represent the directions of the electric vectors. The electric vector map implies an electric displacement loop within the MDM structure, thus, the displacement current in the structure also constructs a loop, which explicitly implies a magnetic resonance. It is noted that the electric nodes for both LSP (FIG. 2 (f) and (g)) and MPP (FIG. 2 (i) and (j)) modes are located within the dielectric gap of the MDM fishnet structure and the mode fields have spatially orthogonal distributions for x- and y-polarizations.

IV. DOUBLE ENHANCEMENT FOR FLUORESCENT EMISSION

A 532 nm linearly polarized laser was used to pump the device. A polarizer and a half-wavelength plate were inserted in front of the MDM fishnet device to control the polarization and maintain constant beam intensity for the incident light. The light was then focused normal on the plane of the sample using an objective lens (10×, NA=0.4, Olympus). By rotating the half-wavelength plate, the polarization angle of the illuminating light can be easily controlled. A 60× oil-immersion objective lens (NA=1.42, Olympus) located underneath the sample was then used to collect the transmitted light, and this light was then reflected by a mirror. A long-pass filter with a cutoff wavelength of 532 nm was used to block any excitation light. An analyzer positioned behind the long-pass filter was used to monitor the polarization of the fluorescent spectrum. The fluorescent spectra were recorded using an automated imaging spectrometer. Finally, the polarization-dependent photoluminescence of Nile Red molecules sandwiched in the gap was measured. A simple view of the experimental set-up is shown in FIG. 3(a). The orientation angles θ for polarizer and φ for analyzer were chosen to be 0° (along x-axis) and 90° (along y-axis), respectively, in the experiments. The fluorescent spectra were obtained using four different polarization combinations, which were denoted by "xx", "xy","yx", and "yy" (see FIG. 3 (b) and (c)). The figures clearly show that the shapes of the enhanced fluorescent emission spectra differ greatly from the intrinsic spectra of Nile Red molecules (see FIG. 1(d)) and are strongly dependent on the orientations of both the polarizer and the analyzer, which indicates strong coupling between fluorescent emitters and plasmonic

DOI:10.1063/1674-0068/cjcp1807182

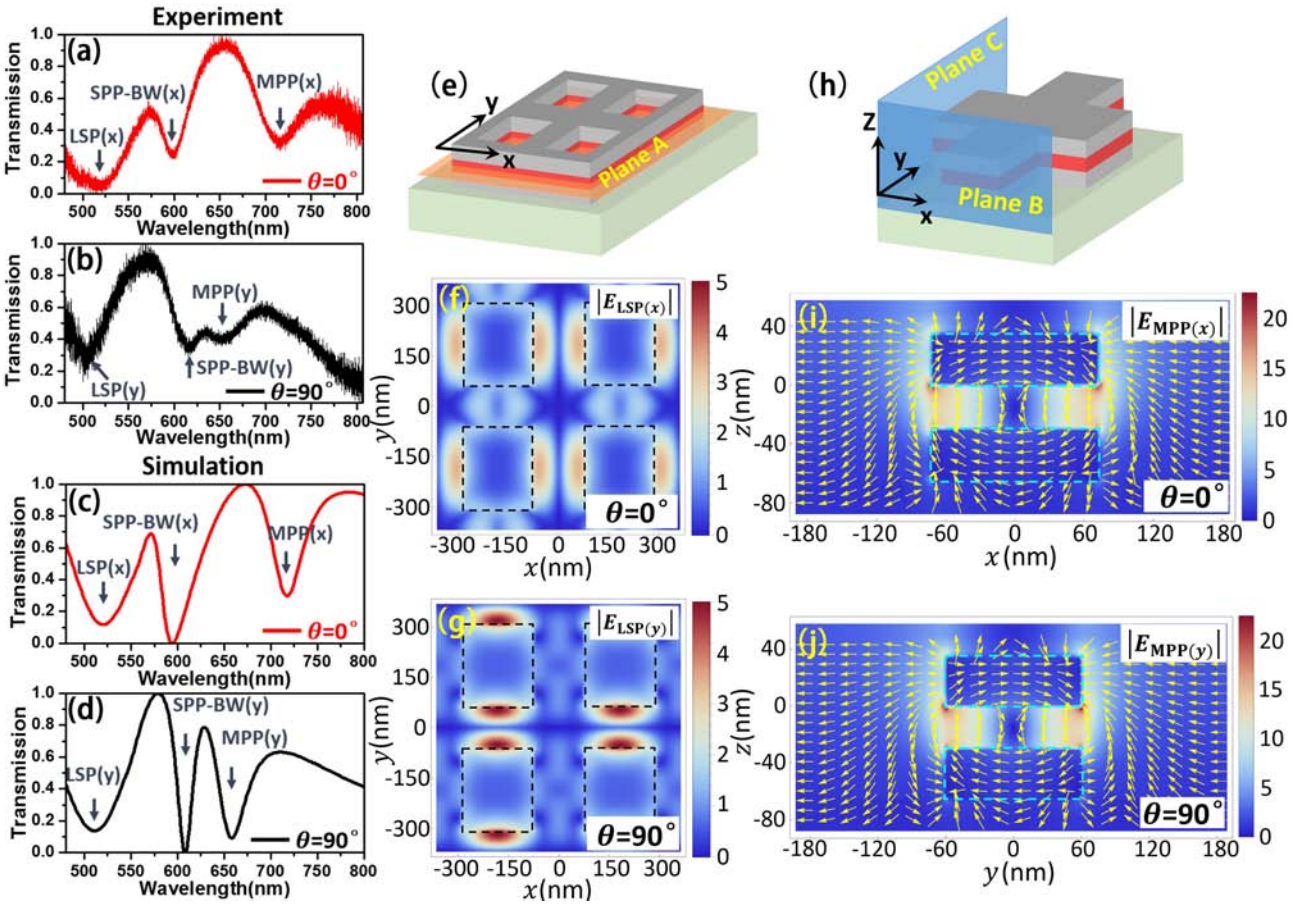

FIG. 2 Linear optical properties of the MDM fishnet structure. (a, b) Experimental and (c, d) simulated transmission spectra of the MDM fishnet structure for incident light polarized in the x- (θ=0°) and y- (θ=90°) directions, respectively. The LSP, SPP-BW and MPP modes for the transverse (x) and longitudinal (y) directions are labeled. (e) Schematic showing detection Plane A (orange plane). (f, g) Electric fields mapped on Plane A for the LSP modes with incident light polarized in (f) x- and (g) y- directions, respectively. The black dashed frames indicate air holes in the fishnet structure. (h) Schematic showing detection Planes B and C (blue planes). (i, j) Electric fields and vectors mapped on (i) Plane B and (j) Plane C for MPP modes. The blue dashed frames indicate silver slabs in the fishnet structure. All the coordinates x, y and z in (f, g, i, j) are corresponding to the coordinate system inserted in (h).

modes of the MDM fishnet structure. The fluorescent emission spectra of the device were measured after the analyzer with x- and y-orientations, as shown in FIG. 3(b) for x-polarized incident laser beam and FIG. 3(c) for y-polarized incident laser beam. When the orientations of the polarizer and the analyzer are parallel, an enhanced fluorescent spectral peak occurs at 715 nm for x-orientation, which corresponds to the resonance wavelength of MPP(x) mode, along with another peak at 645 nm for y-orientation due to MPP(y) mode resonance. It is also noted that the fluorescence spectra still exhibit enhancement, with peaks occurring at 645 nm for x-polarized illumination and 715 nm for y-polarized illumination, in the case where the polarizer and the analyzer are oriented perpendicular to each other.

To clarify the physics behind these enhanced spectra, we conducted FDTD simulations to disclose the excitation and emission coupling behavior between the localized electromagnetic field and the fluorescent emitters. When the broad spectrum of LSP mode is taken into consideration, it is reasonable to expect that the incident 532 nm laser light will induce LSP mode in the MDM fishnet structure. Therefore, the absorption of fluorescent emitter is enhanced by the localized electromagnetic field that occurs in the gap. The electric field distributions at excitation wavelength of 532 nm are inspected at the x-y plane located at the center of the gap (sketched as plane A in FIG. 2(e)). FIG. 3 (d) and (e) show the electric field distributions with incident light polarizations orientated along x- and y-axes, respectively. The field distribution of excitation laser is the same as that of LSP mode (FIG. 2 (f) and (g)). More importantly, the electromagnetic field of the excitation laser has been concentrated efficiently on the subwavelength dielectric gap because of the LSP, and the main lobes of the localized electric field are bounded at

DOI:10.1063/1674-0068/cjcp1807182

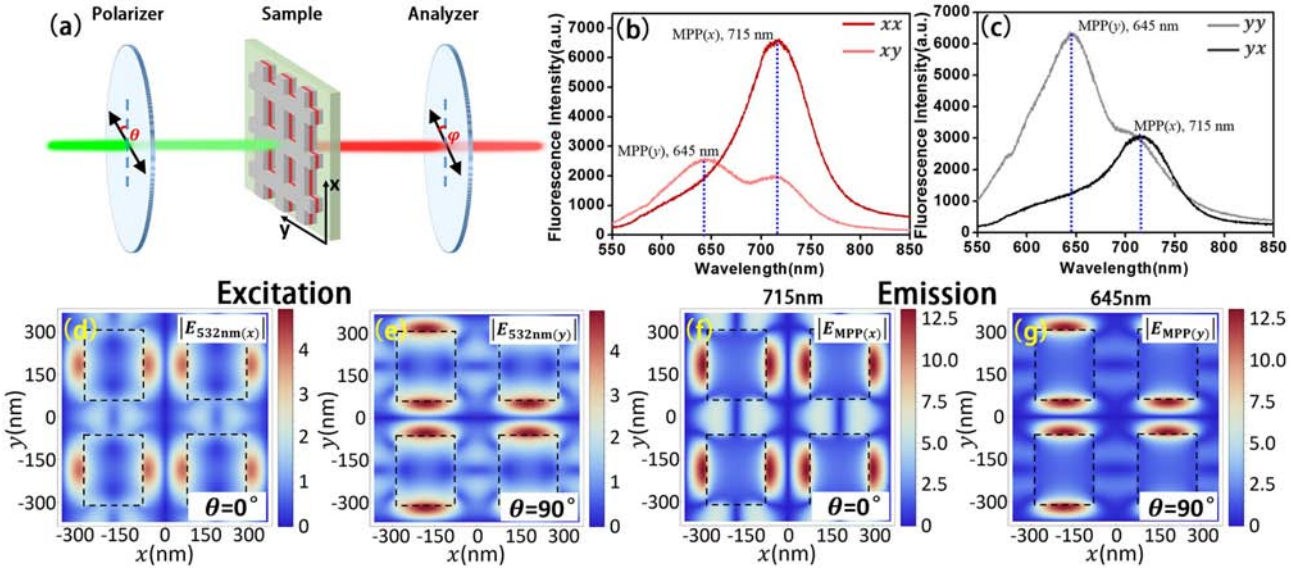

FIG. 3 Fluorescent emission spectra of the structure and electric field distributions of the excitation and emission processes. (a) Simple schematic showing the fluorescence measurement process with varied polarization orientation of both the polarizer and the analyzer. (b, c) Fluorescent spectra for (b) x- (dark and light red curves) and (c) y- (dark and light black curves) excitation polarizations, respectively, when the analyzer polarization axis is aligned parallel (x) and perpendicular (y) to the sample. The MPP modes for x- and y-directions are depicted using blue dot lines. (d, e) Electric fields mapped on Plane A for excitation processes at 532 nm with incident light polarized along (d) x- and (e) y-axis. (f, g) Emission processes at MPP resonance wavelengths of (f) 715 nm (MPP(x)) and (g) 645 nm (MPP(y)). The black dashed frames indicate air holes in the fishnet structure.

the edges along the polarization directions [37]. FIG. 3 (f) and (g) show the electromagnetic field distributions of the MPP modes within the gap, and the main lobes of the localized electromagnetic fields of the LSP and MPP modes overlap with each other in the gap when they have the same polarization. When fluorescent molecules are located at this mode-overlapping site, the coupling of LSP mode with the absorption spectrum of Nile Red molecules and MPP mode with their emission spectrum lead to double enhancement, which accounts for the dramatic enhancement of the fluorescence spectra at 715 nm for "xx" polarization (FIG. 3(b)) and 645 nm for "yy" polarization (FIG. 3(c)). Although the main lobes of the localized electric field at 532 nm are located along the polarization directions, part of the localized electric field are along the perpendicular directions. In consequence, for absorption process, the electric field will excite the fluorescent molecules, both in the orthogonal directions. The analyzer is used to monitor the polarization of the fluorescent spectrum, and thus determine the emission peak. As a result, the enhanced fluorescent spectra for "xy" and "yx" polarizations can both be attributed to partial overlapping of the localized electromagnetic fields of the LSP and MPP modes when they are in different polarizations, which results in single and weak enhancements at the spectrum peaks.

V. POLARIZATION-DEPENDENCE OF THE FLUORESCENT EMISSION

This coupling between plasmonic modes and fluorescent emitters in the MDM fishnet structure can be further corroborated through investigation of the polarization characteristics of the fluorescent emission. To excite all the fluorescent molecules homogeneously within the gap of the MDM fishnet lattice, the device was illuminated using 532 nm laser light with a polarization orientation angle θ=45° and the fluorescence spectra were then recorded at different values of analyzer polarization orientation angle φ over the range from 0° to 90° in steps of 10° (FIG. 4(a)) with equal duration. As a result, MPP(x) (715 nm) and MPP(y) (645 nm) modes were shown to make equivalent contributions to the total fluorescence spectra. Subsequently, we extracted the fluorescent intensities at 715 nm and 645 nm for different analyzer orientation angle φ and plotted the results in FIG. 4 (b) and (c), respectively. When the photobleaching effect [38] is taken into consideration, the dependence of the fluorescence intensity on the orientation angle φ can be fitted well using a cosine function together with an exponential decay [39]. After removing the exponential decay arisen from photobleaching effect, a polar plot of polarization-dependent fluorescence are presented in FIG. 4(d), which gives a straightforward indication of x-polarization of the 715 nm fluorescence (mediated by MPP(x) mode) and y-polarization of the 645 nm fluorescence (mediated by MPP(y) mode). This

DOI:10.1063/1674-0068/cjcp1807182

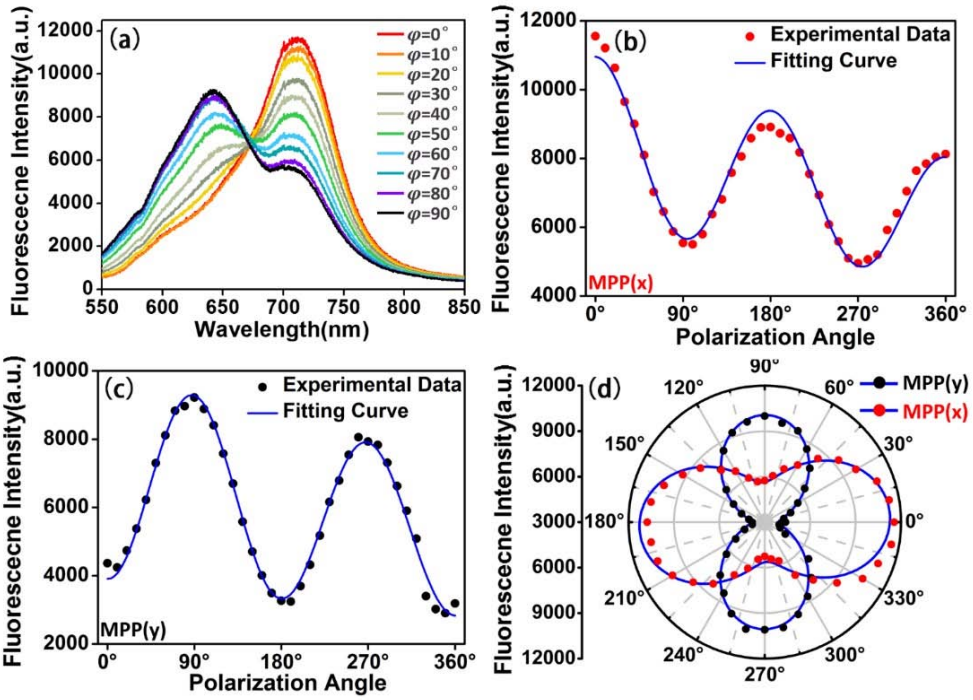

FIG. 4 Polarization dependence of the fluorescent emissions from the MDM fishnet structure. (a) Fluorescence intensity spectra of the structure as analyzer polarization angle φ varies from 0° to 90° in steps of 10° for a fixed excitation angle θ=45°. (b, c) The dependence of fluorescence intensity on the detection polarization angle is shown at (b) 715 nm (solid red circles) and (c) 645 nm (solid black circles) for the sample. The blue curves are fitted to a cosine function together with an exponential decay. (d) Polar plot of the fluorescence intensities (solid red circles and solid black circles, respectively) versus the detection polarization direction as it varies from 0° to 360° in steps of 10°. The data are corrected by removing the exponential decay to indicate the polarizations of the emissions from the sample at 715 nm and 645 nm. The circles and the blue curves are fitted to the cosine function without the exponential decay.

indicates that the polarization-dependent MPP mode enables manipulation of both polarization and wavelength of the fluorescent emission.

To understand these results, we simulated the emission process. Because the localized electric field within the gap at 532 nm is dominated by the z-polarized component, it is reasonable to predict that the fluorescent emission mediated by MPP mode can be simulated by the z-polarized dipole emitter that lies within the gap of the MDM fishnet structure. We therefore considered two representative cases for each emission process. The z-polarized dipole source (yellow cross mark) is located in gap layer near to the left (FIG. 5(a)) and upper (FIG. 5(b)) edge of the rectangular air hole respectively, corresponding to the locations where the electric field of excitation laser is the most intense (FIG. 3 (d, e)). For the case sketched in FIG. 5(a), the simulated far-field distribution components (FIG. 5 (b)–(d) at 715 nm) and the decay rate enhancement (FIG. 5(i)) verify that the far-field radiation mediated by MPP(x) mode is polarized along the x-axis. Similarly, the simulated far-field distribution components (FIG. 5 (f)–(h) at 645 nm) and decay rate enhancement (FIG. 5(j)) for the case sketched in FIG. 5(e) verify that the far-field radiation mediated by MPP(y) mode is mainly y-axis.

VI. CONCLUSION

In conclusion, this work demonstrates that the absorption and emission properties of fluorescent emitters can be enhanced simultaneously using two independent plasmonic modes in an MDM fishnet structure. This double enhancement produces more intense photoluminescent radiation. More importantly, the coupling of the two independent plasmonic modes enables manipulation of the excitation and emission properties of the fluorescent emitters. Use of specific spatial distributions of LSP mode for different polarizations allows the fluorescent molecules dispersed within the gap of the MDM fishnet structure to be excited selectively, which thus enables shaping of the spectrum via tuning of the polarization of excitation laser beam. In addition, the resulting polarization-dependent multimode-mediated emission enables selectivity in terms of both radiation wavelength and polarization. This work opens up the possibility of generation of color light-emitting diodes or laser sources on the nanoscale for use in photonic integrated circuits at visible frequencies.

DOI:10.1063/1674-0068/cjcp1807182

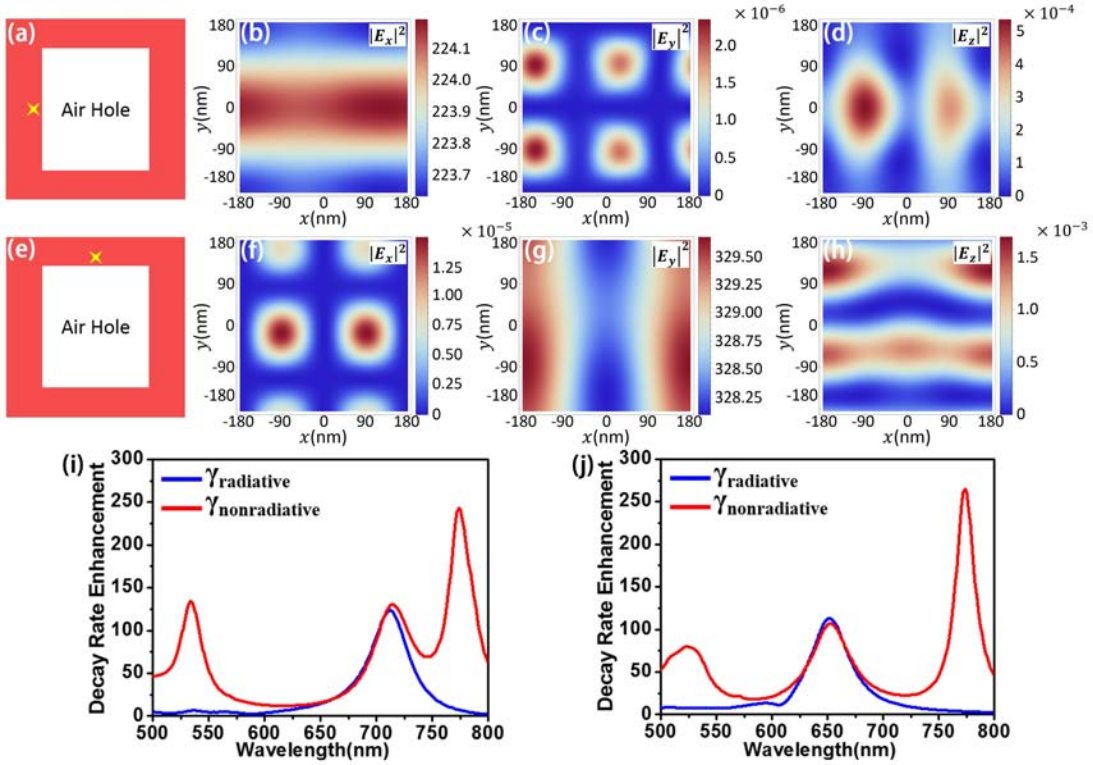

FIG. 5 Electric field distributions in far-field and the corresponding decay rate enhancements. The z-polarized dipole source (yellow cross mark) is located in the gap layer near to (a) left and (e) upper edge of the rectangular air hole. Corresponding x (b, f), y (c, g) and z (d, h) components of the far-field electric field are recorded in the plane 1 μm below the sample surface at 715 nm (MPP(x)) and 645 nm (MPP(y)), respectively. (i, j) Simulated decay rate enhancements with radiative peak of (i) 715 nm, and (j) 645 nm for the dipoles sketched in (a) and (e), respectively.

VII. ACKNOWLEDGEMENTS

This work was supported by the National Nature Science Foundation of China (No.11674303 and No.11574293), and the USTC Center for Micro and Nanoscale Research and Fabrication.

[1] M. Pelton, Nature Photon. **9**, 427 (2015).
[2] J. A. Schuller, E. S. Barnard, W. Cai, Y. C. Jun, J. S. White, and M. L. Brongersma, Nat. Mater. **9**, 193 (2010).
[3] O. Hess, J. B. Pendry, S. A. Maier, R. F. Oulton, J. M. Hamm, and K. L. Tsakmakidis, Nat. Mater. **11**, 573 (2012).
[4] K. L. Tsakmakidis, R. W. Boyd, E. Yablonovitch, and X. Zhang, Opt. Express **24**, 17916 (2016).
[5] D. Wei, S. Chen, and Q. Liu, Appl. Spectrosc. Rev. **50**, 387 (2015).
[6] L. Zhao, T. Ming, H. Chen, Y. Liang, and J. Wang, Nanoscale **3**, 3849 (2011).
[7] P. Bharadwaj and L. Novotny, Opt. Express **15**, 14266 (2007).
[8] M. Ringler, A. Schwemer, M. Wunderlich, A. Nichtl, K. Kurzinger, T. A. Klar, and J. Feldmann, Phys. Rev. Lett. **100**, 203002 (2008).
[9] A. Kinkhabwala, Z. F. Yu, S. H. Fan, Y. Avlasevich, K. Mullen, and W. E. Moerner, Nature Photon. **3**, 654 (2009).
[10] X. Meng, R. R. Grote, J. I. Dadap, N. C. Panoiu, and R. M. Osgood, Opt. Express **22**, 22018 (2014).
[11] R. Guo, S. Derom, A. I. Vakevainen, R. J. van Dijk-Moes, P. Liljeroth, D. Vanmaekelbergh, and P. Torma, Opt. Express **23**, 28206 (2015).
[12] K. Li, K. Jiang, L. Zhang, Y. Wang, L. Mao, J. Zeng, Y. Lu, and P. Wang, Nanotechnology **27**, 165401 (2016).
[13] A. Rose, T. B. Hoang, F. McGuire, J. J. Mock, C. Ciraci, D. R. Smith, and M. H. Mikkelsen, Nano Lett. **14**, 4797 (2014).
[14] Q. Y. Lin, Z. Y. Li, K. A. Brown, M. N. O'Brien, M. B. Ross, Y. Zhou, S. Butun, P. C. Chen, G. C. Schatz, V. P. Dravid, K. Aydin, and C. A. Mirkin, Nano Lett. **15**, 4699 (2015).
[15] A. Abass, SRK. Rodriguez, T. Ako, T. Aubert, M. Verschuuren, D. V. Thourhout, J. Beeckman, Z. Hens, J. G. Rivas, and B. Maes, Nano Lett. **14**, 5555 (2014).
[16] Z. K. Zhou, D. Y. Lei, J. M. Liu, X. Liu, J. C. Xue, Q. Z. Zhu, H. J. Chen, T. R. Liu, Y. Y. Li, H. B. Zhang, and X. H. Wang, Adv. Opt. Mater. **2**, 56 (2014).
[17] M. Parzefall, P. Bharadwaj, A. Jain, T. Taniguchi, K. Watanabe, and L. Novotny, Nat. Nanotechnol. **10**, 1058 (2015).
[18] S. Xiao, V. P. Drachev, A. V. Kildishev, X. Ni, U. K.

Chettiar, H. K. Yuan, and V. M. Shalaev, Nature **466**, 735 (2010).
[19] A. Fang, T. Koschny, and C. M. Soukoulis, Phys. Rev. B **82** (2010).
[20] J. M. Hamm, S. Wuestner, K. L. Tsakmakidis, and O. Hess, Phys. Rev. Lett. **107**, 167405 (2011).
[21] E. M. Larsson, J. Alegret, M. Kall, and D. S. Sutherland, Nano Lett. **7**, 1256 (2007).
[22] Y. Liu, J. Bishop, L. Williams, S. Blair, and J. Herron, Nanotechnology **15**, 1368 (2004).
[23] I. H. El-Sayed, X. Huang, and M. A. El-Sayed, Nano Lett. **5**, 829 (2005).
[24] M. R. Gartia, A. Hsiao, M. Sivaguru, Y. Chen, and G. L. Liu, Nanotechnology **22**, 365203 (2011).
[25] X. Yang, P. L. Hernandez, C. Dang, E. Mutlugun, K. Zhang, H. V. Demir, and X. W. Sun, Adv. Opt. Mater. **3**, 1439 (2015).
[26] J. Pan, J. Chen, D. Zhao, Q. Huang, Q. Khan, X. Liu, Z. Tao, Z. Zhang, and W. Lei, Opt. Express **24**, A33 (2016).
[27] H. A. Atwater and A. Polman, Nat. Mater. **9**, 205 (2010).
[28] J. H. Song, T. Atay, S. Shi, H. Urabe, and A. V. Nurmikko, Nano Lett. **5**, 1557 (2005).
[29] M. Ramezani, A. Halpin, A. I. Fernández-Domínguez, J. Feist, S. R. K. Rodriguez, F. J. Garcia-Vidal, and J. Gómez Rivas, Optica **4**, 31 (2016).
[30] H. Aouani, O. Mahboub, E. Devaux, H. Rigneault, T. W. Ebbesen, and J. Wenger, Nano Lett. **11**, 2400 (2011).
[31] H. Chen, T. Ming, L. Zhao, F. Wang, L. D. Sun, J. Wang, and C. H. Yan, Nano Today **5**, 494 (2010).
[32] C. Belacel, B. Habert, F. Bigourdan, F. Marquier, J.-P. Hugonin, S. Michaelis de Vasconcellos, X. Lafosse, L. Coolen, C. Schwob, C. Javaux, B. Dubertret, J.-J. Greffet, P. Senellart, and A. Maitre, Nano Lett. **13**, 1516 (2013).
[33] X. Li, F. J. Kao, C. C. Chuang, and S. He, Opt. Express **18**, 11335 (2010).
[34] C. L. Haynes and R. P. Van Duyne, J. Phys. Chem. B **107**, 7426 (2003).
[35] C. Zhang, Y. Lu, Y. Ni, M. Li, L. Mao, C. Liu, D. Zhang, H. Ming, and P. Wang, Nano Lett. **15**, 1382 (2015).
[36] E. D. Palik, *Handbook of Optical Constants of Solids*, Vol.3, New York: Academic press, (1998).
[37] Y. Ren, Y. Lu, T. Zang, Y. Wang, Y. Dai, and P. Wang, Opt. Express **25**, 28417 (2017).
[38] A. Diaspro, G. Chirico, C. Usai, P. Ramoino, and J. Dobrucki, *Handbook of Biological Confocal Microscopy*, New York: Springer, 690 (2006).
[39] T. Ming, L. Zhao, Z. Yang, H. Chen, L. Sun, J. Wang, and C. Yan, Nano Lett. **9**, 3896 (2009).

DOI:10.1063/1674-0068/cjcp1807182